Analysis of Multiple Input Multiple Output-Orthogonal Frequency Division Multiplexing with Dynamic Optimal Power Allocation

Owk Srinivasulu
Department of Electronics and Communication Engineering, Andhra University, Vizag, India
srinivasulu.owk@gmail.com (corresponding author)

P. Rajesh Kumar
Department of Electronics and Communication Engineering, Andhra University, Vizag, India
rajeshauce@gmail.com

Received: 19 April 2024 | Revised: 17 May 2024 | Accepted: 193 May 2024

 DOI: https://doi.org/10.48084/etasr.7459

ABSTRACT

Multiple Input Multiple Output (MIMO) is a technology that combines multiple antennas and Orthogonal Frequency Division Multiplexing (OFDM) modulation to increase the data rate and spectral efficiency of wireless communication systems. Equalization problems are one of the key issues with MIMO-OFDM systems, which are caused by multiple antennas and subcarriers. Optimal Power Allocation (OPA) in MIMO-OFDM is a critical component for achieving high spectral efficiency and improving the overall performance of the system. OPA refers to the process of allocating power to the different subcarriers and antennas in MIMO-OFDM systems in an optimal way. This study proposes the Dynamic OPA (DOPA) algorithm for MIMO-OFDM systems to dynamically adjust power allocation based on the changing channel conditions and reduce pilot contamination issues. This approach allocates more power to subcarriers and antennas with better channel conditions and less power to subcarriers and antennas with worse channel conditions. DOPA in MIMO-OFDM systems is necessary to maximize data rates, minimize interference, improve system capacity, and reduce power consumption. Simulation results showed that the proposed MIMO-OFDM-DOPA had reduced bit error rates, mean square error, and transmitter power and increased energy efficiency and capacity compared to existing state-of-the-art methods.

Keywords-multiple input multiple output; orthogonal frequency division multiplexing; dynamic optimal power allocation; energy efficiency; transmit power

I. INTRODUCTION

MIMO-OFDM [1] is a popular wireless communication method that uses multiple antennas and subcarriers to improve system performance. One of the challenges in MIMO-OFDM systems is the optimal allocation of power to each subcarrier and antenna, which affects the system's capacity, spectral efficiency, and error rate [2-8]. There are various power allocation strategies for MIMO-OFDM systems, such as water-filling, channel inversion, and fixed power allocation. The water-filling strategy allocates power to subcarriers based on their channel gains and noise power, while the channel inversion strategy allocates equal power to all subcarriers [9-11]. The fixed power allocation strategy allocates equal power to each subcarrier regardless of their channel gains [12]. The choice of power allocation strategy depends on the specific requirements of the wireless communication system, such as the number of antennas, the signal-to-noise ratio, and the capacity constraints [13, 14].

OPA allocates power to subcarriers and antennas based on specific optimization criteria, such as maximizing the system capacity, minimizing the error rate, or maximizing spectral efficiency [15]. Sub-OPA strategies are simpler and less computationally intensive than OPA [16], as they allocate power based on heuristics or approximations of optimization criteria. Examples of sub-OPA strategies include equal power allocation [17], proportional fairness, and geometric mean decomposition. In practice, a combination of power allocation strategies can be used to achieve optimal system performance. Accurate CSI is required to optimize power allocation [18]. CSI feedback involves transmitting information about the channel from the receiver back to the transmitter. The accuracy of the CSI feedback depends on the frequency and amount of feedback and the power estimation algorithm. In multiuser MIMO-OFDM systems, interference between users can affect OPA [19].

II. THE PROPOSED METHOD

Figure 1 suggests a MIMO-OFDM setup, with T transmit and R receive antennas using DOPA signals modulated with Quadrature Phase Shift Keying (QPSK). In this scenario, imagine sending a time-domain block signal of length N, having the form $\{X_n;\ n = 0,1 \dots, N-1\}$. The consistent frequency-domain block can be found using the Discrete Fourier Transform (DFT) on the time-domain block. The formula for this is $\{X_k;\ k = 0,1,\dots,N-1\} = DFT\{x_n;\ n = 0,1,\dots,N-1\}$. When the repeated prefix is removed and an assumed repeated prefix that is larger than the full network impulse response is applied, the occurrence area representation of the received signal is:

$$Y_k = X_k H_k + N_k \quad (1)$$

The frequency response of the channel for the k^{th} subcarrier can be calculated using $\{H_k; k = 0,1,\dots,N-1\} = DFT\{h_n; n = 0,1,\ \dots,\ N-1$. This formula is assumed to remain constant throughout the transmission of a given block. In addition, in the frequency domain, the symbol N_k denotes the block channel noise for the defined subcarrier. When (1) is applied to the received time-domain signal it can be determined: $\{y_n;\ n = 0,1,\dots,N-1\} = IDFT\{Y_k;\ k = 0,1,\dots,N-1\}$.

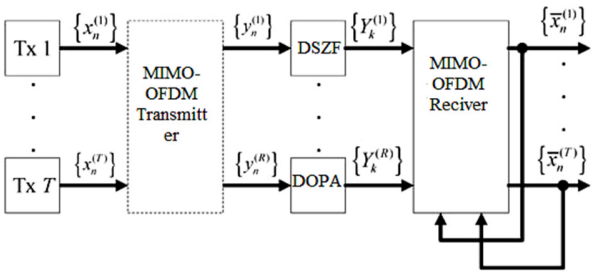

Fig. 1. Block diagram of MIMO-OFDM with DOPA signals.

Since traditional linear FDEs are always used in SC schemes, the subsequent processing consists of:

$$X\tilde{}k = [Y_k\ H_k]\beta_k^{(2)} \quad (2)$$

where $\beta_k^{(2)} = \left(\alpha + (|H_k|^2)\right)^{-1}$. Therefore:

$$X\tilde{}k = X_k\ |H_k|2\beta_{(2)k} + N_{keq} \quad (3)$$

This indicates that the symbol received is identical to the one transmitted, except that it has undergone a gradient of $|H_k|2$, a noise factor of $\beta_k^{(2)}$, and additional noise of N_{keq}.

$$\alpha = E[|N_k|^2/[E|X_k|]^2] \quad (4)$$

where N_k^{eq} denotes the corresponding noise for recognition determination, with $E[\left|N_k^{eq}\right|^2] = [2\sigma_N^2\ |H_k|^2]\beta_k^{(2)}$ and $\sigma_N^2 = E\ {[|N_k|^2]}/{2}$. The concept that the t^{th} antenna has a collection of N data symbols that it needs to send out into the world is denoted by $\{x_n^{(t)};\ n = 0,1 \dots, N-1\}$. The content of the block that was transmitted by the r^{th} user to the BS is denoted by $\{y_n^r;\ k = 0,1,\dots,N-1\}$. The beginning of each block sent, in the same manner as in prior DOPA systems, has a cyclic sequence appended to it that is longer than the maximum total channel impulse response. This is done to ensure that the block can be decoded successfully. When it comes to this situation, the recipient won't pay any heed to the prefix. This approach proceeds under the premise that the portion of the frequency domain denoted by $\{Y_k^{(r)};\ k = 0,1,\dots,N-1\}$ satisfies the conditions specified.

$$Y_k = \left[Y_k^{(1)}, \dots\dots, Y_k^{(R)}\right]^T = H_k X_k + N_k \quad (5)$$

where H_k is the $T{\times}R$ channel matrix for the k^{th} frequency, $H_k^{(t,r)}$ is the element that corresponds to the $(r,\ t)^{\text{th}}$ frequency, and $H_k^{(t,r)}$ represents the k^{th} frequency. The formula for the sent symbols is $X_k = \left[X_k^{(1)}, \dots., X_k^{(T)}\right]^T$.

The estimated data symbols in the frequency domain are represented by $X_k\tilde{}=\left[X_k^{\sim(1)}, \dots, X_k^{\sim(R)}\right]^T$. These symbols can be found by looking at the frequency domain. If the receiver does not engage in iteration, the following options are available: Here, $H_k^{(t,r)}$ is the element that corresponds to the $(r,\ t)^{\text{th}}$ frequency. The TR frequency medium for the k^{th} frequency is expressed as $X_k = \left[X_k^{(1)}, \dots., X_k^{(T)}\right]^T$. For the estimated data symbols in the frequency domain, $X_k^{\sim} = \left[X_k^{\sim(1)}, \dots, X_k^{\sim(R)}\right]^T$, the following apply if the recipient is not iterative:

$$X_k^{\sim} = B_k Y_k \quad (6)$$

where B_k is an unknown constant, whose value depends on the following:

Step 1: Consider DSZF

$$B_k = (H_k^H H_k)^{-1} H_k^H \quad (7)$$

Step 2: The MRC receiver can be used in the following situations:

$$B_k = H_k^H \quad (8)$$

Step 3: by the EGC receiver, as:

$$B_k = \exp\{j\ arg(H_k^H)\} \quad (9)$$

The DSZF requires a high-powered computer to calculate the pseudo-inverse of the network medium for each occurrence factor. The DSZF needs this because it uses the Z-transform. Applying the MRC and EGC algorithms can work around this limitation. When R is equal to one and there is only a modest correlation between the channels supplied by the various transmitting and receiving antennas, the elements of the MIMO-OFDM matrix that are not on the main diagonal are ignored.

$$temp = A_k^H H_K \quad (10)$$

where, $[A]_{i,i}\ '= [H]_{i,i}^H$ is a notation used inside the MRC framework. Since $[A]_{i,i'} = exp(j\ arg([H]_{i,i'}))$, the absolute value is 1 and the phase is the same as the member of the matrix H that corresponds to it. The MRC or EGC can be used in the frequency domain by exploiting the relationship

between $A_k^H H_k$. As a result, there may be some residual interference present, even at tolerable values of *T/R*. The iterative receiver, also known as an interference canceller, has been designed to deal with this problem.

$$X_k^{\sim} = B_k^H Y_k - C_k X_k^{-} \quad (11)$$

The expected data's frequency domain symbols are denoted by $X_k^{\sim} = \left[X_k^{\sim(1)}, \ldots, X_k^{\sim(R)}\right]^T$, and the interfering termination matrix C_k can be found by:

$$C_k = A_k^H H_k - I \quad (12)$$

To create an interference canceller, the formula $\bar{X}_k = [\bar{X}_0, \ldots, \bar{X}_{N-1}]$ can be used, where $\bar{X}_k$ represents the average value in the frequency domain in comparison to the output of the FDE in the iteration before this one. The formula in [20] can be used to determine $\bar{X}_n$. For the initial cycle, $\bar{X}_k = 0$, as the transmitted symbols cannot be predicted.

A. DOPA Analysis

The traditional form of pilots is used to prevent any unnecessary repetition of training data. Traditional training sequence pilots have the sender send out a series of known symbols at regular intervals so the receiver can estimate the channel parameters required for equalization, as shown in Figure 2. Under these conditions, an approximation of the network's occurrence comeback can be made with the following formula:

$$H_k^{\sim(t,r)} = \frac{Y_k^{(r)} X_k^{(t)P*}}{2\sigma_p^2} \quad (13)$$

where $r = 1, 2$ represents the positions of the receiving antennas, and $Y_k^{(r)}$ is the signal at the r^{th} receiving antenna, while $X_k^{(t)P}$ is the pilot transmitted by the t^{th} transmitting antenna ($t = 1,2, \ldots, T$). The training sequences σ_p^2 are a representation of the pilots' strengths (*P* stands for the pilot).

$$\sigma_P^2 = E\left\{\left|X_k^p\right|^2\right\}/_2 = NE\left\{|x_n^P|^2\right\}/_2 \quad (14)$$

When the channels that each transmit antenna corresponds to are computed, there will not be any interference if the pilots that connect them are orthogonal.

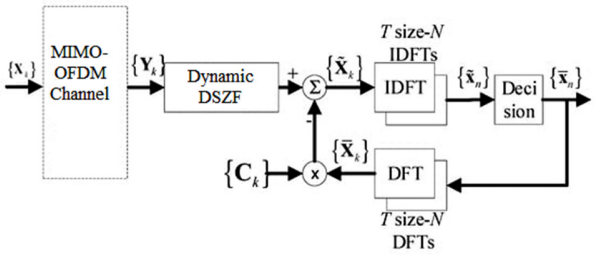

Fig. 2. Block diagram of MIMO-OFDM with DPOA.

$$X_k^{P(m)} X_k^{P(q)*} = 0, \quad m \neq q \quad (15)$$

Then the channel instinct reply is much quicker than the cyclic prefix, which is only a small portion of the total period of the block. This study uses the enhanced power estimates in the form of [21]. This is because the cyclic prefix is only a small portion of the total period of the block.

$$H_k^{(t,r)} = DEF\left\{h_n^{\sim(t,r)} w_n\right\} \quad (16)$$

where $w_n = 1$ if the n^{th} time-domain example is contained within the cyclic prefix and 0 if it is not contained within the prefix. In this scenario, the SNR at a factor expressed by *T/TG*, where *T* and *TG* represent the duration of the channel's usable block section and the cyclic prefix, respectively, the estimations of the channel's characteristics are enhanced. For the subcarriers that currently have pilots installed, superimposed pilots can be introduced, often known as X_k^0. With MIMO-OFDM, spectral efficiency is degraded because of the increased complexity of DOPA using traditional pilot symbols. The suppression offered by the overlaid pilots helps to lower these costs and improves spectral efficiency.

$$\sigma_D^2 = E\ \{|X_k|^2\}/2 = NE\ \{|x_n|^2\}/2 \quad (17)$$

where σ_D^2 is the magnitude of the data. Suppose a frame that has *NT* time-domain blocks, each of them having *N* subcarriers. If the cyclic prefix of each FFT block has $NG = NTG/T$ samples, then the power estimate requires *NG* equally spaced frequency-domain pilots. The number of pilots in the frame can be calculated using the time and frequency parameters, *NT* and *NF*, respectively. As a result, the goal can be accomplished.

$$N_P^{Frame} = \frac{N}{\Delta NF} \cdot \frac{N_T}{\Delta N_T} \quad (18)$$

This means that pilot diversity or redundancy is:

$$N_R = \frac{N_p^{Frame}}{N_G} = \frac{N}{N_G \Delta N_F} \cdot \frac{N_T}{\Delta N_T} \quad (19)$$

The signal-to-noise ratio (SNR) that is related to the DOPA, denoted by $SNR_{est} \approx N\ {R\sigma_P^2}/{\sigma_D^2}$, should be significantly higher than the SNR associated with the data, denoted by $SNR_{data} = {\sigma_D^2}/{\sigma_N^2}$, to prevent significant performance degradation brought on by errors in DOPA. If superimposed pilots (pilots added to data) are present, both the data and the pilots would serve as representations of interference to the DOPA that would otherwise be acquired from the data. Since the data and the pilots introduce noise into the DOPA, performance will suffer.

The first step involves collecting the pilots' power estimates (if this is not the first iteration, clear the data beginning with the received signal collected in the previous iteration). The second step removes the pilots (an indication of interference) from the received signal before utilizing the data to generate power estimates. Step three requires combining the estimates of the channel obtained in the first and second steps to create a more exact estimate of the channel. Using the correlation between the Rx signal $Y_k^{(r)Rz}$ and the pilots, a first-pass power estimate

can be generated for the first iteration (step 1). Getting a true picture of the channel requires this extra step. The following procedure is used to clear the received blocks of data symbols.

$$Y_k^{(r)P} = Y_k^{(r)Rx} - Y_k^{(r)D} = Y_k^{(r)Rx} - H_k^{\sim(t,r)} X_k^{\sim(t)} \quad (20)$$

where an estimation of the channel can be obtained by applying (13) and (16). The pilots are removed from the blocks received in the second iteration (the second phase).

$$Y_k^{(r)D} = Y_k^{(r)Rx} - Y_k^{(r)P} = Y_k^{(r)Rx} - H_k^{\sim(t,r)} X_k^{(t)P} \quad (21)$$

The data symbols' median values are used as guides to estimate the channel's frequency response. This can determine the channel's occurrence response.

$$H_k^{\sim(i)(t,r)D} = \frac{Y_k^{(i-1)(r)D} X_k^{\sim(i-1)(t)*}}{\left|X_k^{\sim(i-1)(t)}\right|^2 + \alpha} \quad (22)$$

Because setting has the potential to have noise improvement in the network estimates when $\left|X_k^{(i)}\right|^2$ is low, the specification in (4) is followed. If SNR is moderate to high, then:

$$\left|X_k^{(i)}\right|^2 \approx 2\sigma_P^2 \quad (23)$$

The equation $\alpha = 0$ can be used. This approach chooses pilots that had power on the lower end of the spectrum, and to acquire precise DOPAs, the pilots were normalized over many blocks. As it is important to maintain a steady channel output, this window limitation is obligatory. After step 3 is finished, the normalized power estimates with the smallest error variance [14] are obtained by integrating the pilot ($H_k^{\sim P}$) and the data ($H_k^{\sim D}$) power estimates.

$$H_k^{\sim P,D} = \frac{\sigma_D^2 H_k^{\sim P} + \sigma_p^2 H_k^{\sim D}}{\sigma_D^2 + \sigma_p^2} = H_k + \varepsilon_k^{P,D} \quad (24)$$

$$\left[\left|\varepsilon_K^{P,D}\right|^2\right] = \sigma_{P,D}^2 = \frac{\sigma_D^2 \sigma_p^2}{\sigma_D^2 + \sigma_p^2} \quad (25)$$

III. RESULTS AND DISCUSSION

The simulation of the MIMO-OFDM system using a DSZF equalizer was implemented in Matlab R2018a.

A. Simulation Parameters

Table I presents the simulation parameters.

TABLE I. SIMULATION PARAMETERS

Parameters	Value
Number of BS antennas	4, 8, 16
Number of pilots	10000
Channel sparsity	60
Channel type	Rician
Signal-to-Noise ratio range	0-30 dB
FFT size	128
System bandwidth	20 MHz
Carrier frequency	2.6 GHz

The non-zero coefficients in the channel generate a Gaussian compound distribution with zero mean and unit variance. Rician fading is a stochastic model for radio propagation anomalies caused by the partial cancelation of a DSZF signal by itself. The signal arrives at the receiver via several different paths (exhibiting multipath interference), and at least one of the paths is changing. Rician fading is caused by the partial cancelation of a DSZF signal by itself (lengthening or shortening). Rician fading happens when one of the pathways is often a signal traveling in line-of-sight or some strong reflection signals. The amplitude gained in Rician fading may be thought of as having a Rician distribution as its defining feature.

B. BER Performance Evaluation

Figures 3, 4, and 5 present the BER performance of 4×4, 8×8, and 16×16 MIMO systems, respectively. The BER values are measured in the range of 0-8 dB of SNR. The proposed MIMO-OFDM approach resulted in reduced BER compared to conventional approaches. Figure 3 shows that the MIMO-MAPSO method resulted in a BER of 10^{-6} at 5 dB, SLM-PTS had 10^{-6} at 8 dB, CFIM-MIMO-FSO and MIMO-OFDM-STBC had 10^{-4} at 8 dB, FWGO-GPTR-PTS had 10^{-6} at 3.6 dB, and MIMO-OFDM-DSZF had 10^{-6} at 2.9 dB. The proposed MIMO-OFDM resulted in a reduced BER of 10^{-6} at 2.6 dB, which was less compared to the other approaches.

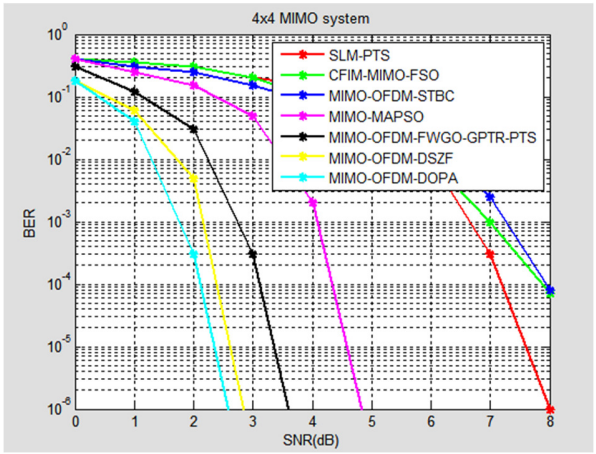

Fig. 3. BER performance of 4×4 MIMO-OFDM systems.

Figure 4 shows that the conventional SLM-PTS method had a BER of 0.01 at 8 dB, CFIM-MIMO-FSO had 2×10^{-5} at 8 dB, MIMO-OFDM-STBC had 10^{-6} at 6.2 dB, MIMO-MAPSO method had 10^{-6} at 5.5dB, MIMO-OFDM-FWGO-GPTR-PTS had 10^{-6} at 5 dB, and MIMO-OFDM-DSZF had 10^{-6} at 3.7 dB. The proposed MIMO-OFDM-DOPA had a BER of 10^{-6} at 2.9 dB, which was less compared to the other approaches.

Figure 5 shows that the conventional SLM-PTS method had a BER of 0.03 at 8 dB, CFIM-MIMO-FSO had 2×10^{-4} at 8 dB, MIMO-OFDM-STBC had 2×10^{-5} at 8 dB, MIMO-MAPSO had 10^{-5} at 8dB, MIMO-OFDM-FWGO-GPTR-PTS had 10^{-6} at 6.2 dB, and MIMO-OFDM-DSZF had 10^{-6} at 5.4 dB. The proposed MIMO-OFDM-DOPA had a BER of 10^{-6} at 4.2 dB, which was less compared to the other approaches.

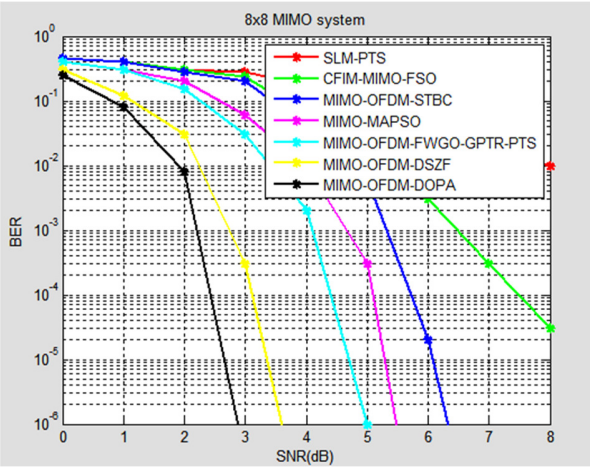

Fig. 4. BER performance of 8×8 MIMO-OFDM systems.

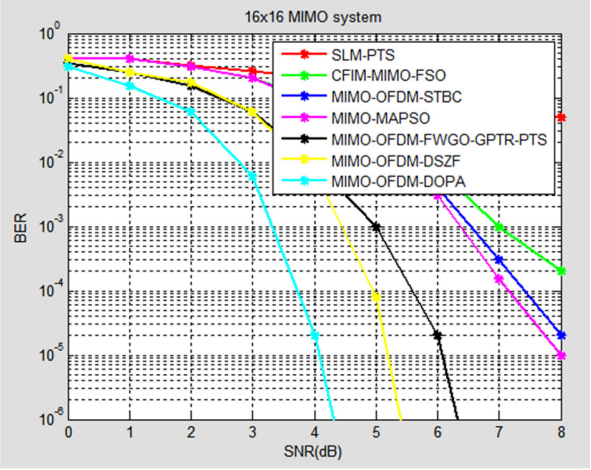

Fig. 5. BER performance of 16×16 MIMO-OFDM systems.

C. MSE Performance Evaluation

Figures 6, 7, and 8 present the MSE performance of 4×4, 8×8, and 16×16 MIMO-OFDM systems, measured in the range of 0-30 dB of SNR. The proposed MIMO-OFDM-DOPA approach had less MSE compared to conventional approaches. Figure 6 shows that the conventional CFIM-MIMO-FSO method had 5×10^{-3} MSE at 30 dB, SLM-PTS had 2×10^{-3} at 30dB, MIMO-MAPSO had 10^{-3} at 18 dB, MIMO-OFDM-STBC had 10^{-3} at 23 dB, EHPTS had 10^{-3} at 27.5 dB, FWGO-GPTR-PTS had 10^{-3} at 20 dB, and MIMO-OFDM-DSZF had 10^{-3} at 18 dB. The proposed MIMO-OFDM-DOPA approach had an MSE of 10^{-3} at 14 dB.

Figure 7 shows that the conventional CFIM-MIMO-FSO method had an MSE of 2×10^{-3} at 30 dB, SLM-PTS had 10^{-3} at 28 dB, MIMO-MAPSO had 10^{-3} at 26 dB, MIMO-OFDM-STBC had 10^{-3} at 23.5 dB, EHPTS had 10^{-3} at 22 dB, FWGO-GPTR-PTS had 10^{-3} at 20 dB, and MIMO-OFDM-DSZF had 10^{-3} at 19 dB. The proposed MIMO-OFDM-DOPA had an MSE of 10^{-3} at 14.5 dB, which was less compared to the other approaches.

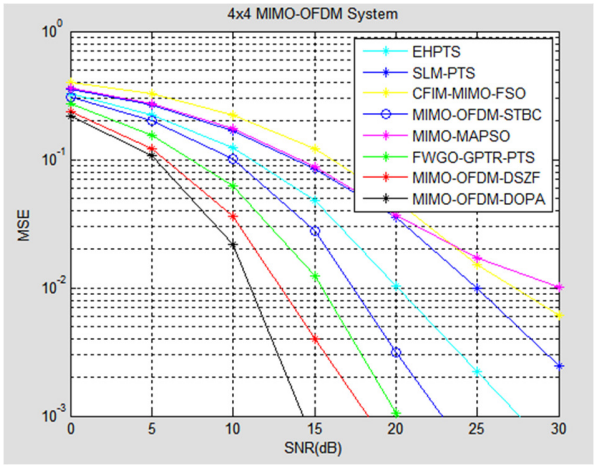

Fig. 6. MSE performance of 4×4 MIMO-OFDM systems.

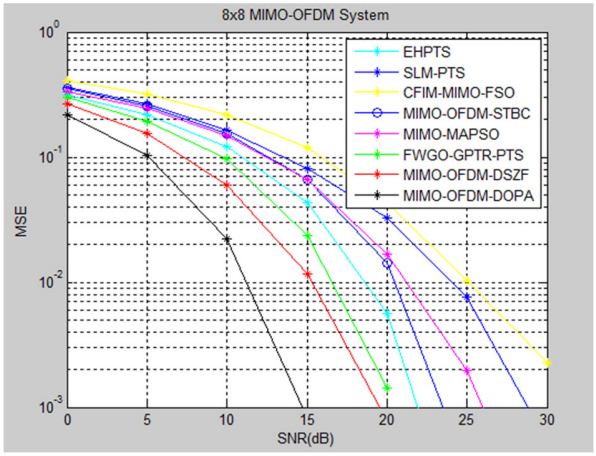

Fig. 7. MSE performance of 8×8 MIMO-OFDM systems.

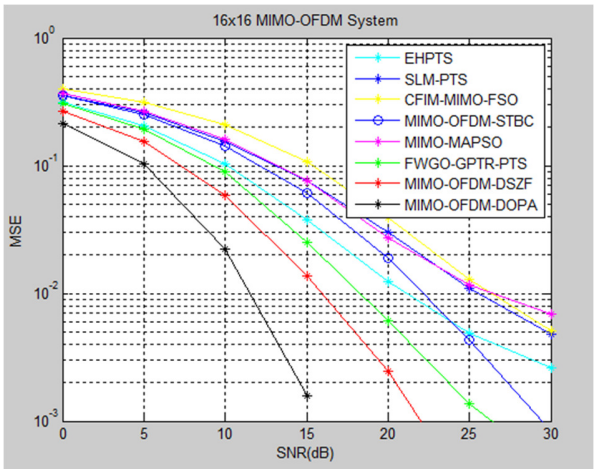

Fig. 8. MSE attainment of 16×16 MIMO-OFDM systems.

Figure 8 shows that the conventional CFIM-MIMO-FSO method had an MSE of 5×10^{-5} at 34 dB, SLM-PTS had 10^{-3} at 30 dB, MIMO-MAPSO had 10^{-3} at 30 dB, MIMO-OFDM-STBC had 10^{-3} at 29 dB, EHPTS had 3×10^{-3} at 30 dB, FWGO-GPTR-PTS had 10^{-5} at 26 dB, and MIMO-OFDM-DSZF had

10^{-5} at 22 dB. The proposed MIMO-OFDM-DOPA had an MSE of 10^{-3} at 15 dB, which was less compared to the other approaches.

D. Energy Efficiency Evaluation

Figure 9 shows the energy efficiency performance of various MIMO-OFDM systems for 250 UEs. TSCE resulted in 3.5 MBPJ of energy efficiency, LDLH had 4.1 MBPJ, DMH-LQE had 4.5 MBPJ, FWGO-GPTR-PTS had 4.8 MBPJ and MIMO-OFDM-DSZF had 6 MBPJ. The proposed MIMO-OFDM-DOPA-DSZF resulted in increased energy efficiency with 8 MBPJ, which was better than the other methods. Figure 10 shows the capacity performance of various MIMO-OFDM systems for 250 UEs. TSCE resulted in a 2.5 MBPS capacity, LDH had 3.8 MBPS, DMH-LQE had 3 MBPS, FWGO-GPTR-PTS had 3.2 MBPS and MIMO-OFDM-DSZF had 6 MBPS. The proposed MIMO-OFDM-DOPA resulted in 9.8 MBPS channel capacity, which was higher compared to the other methods.

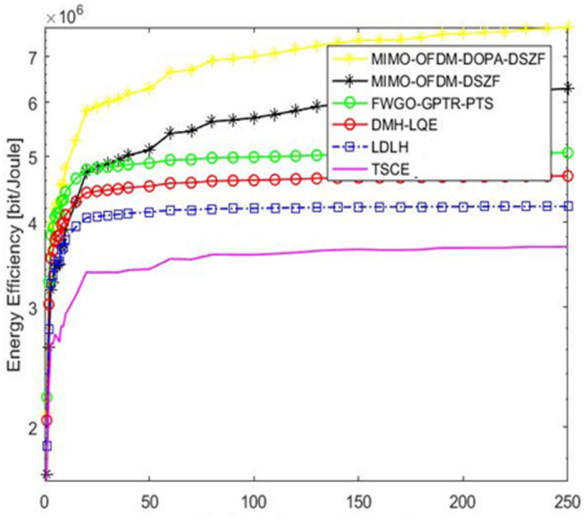

Fig. 9. Energy efficiency performance of various MIMO-OFDM systems.

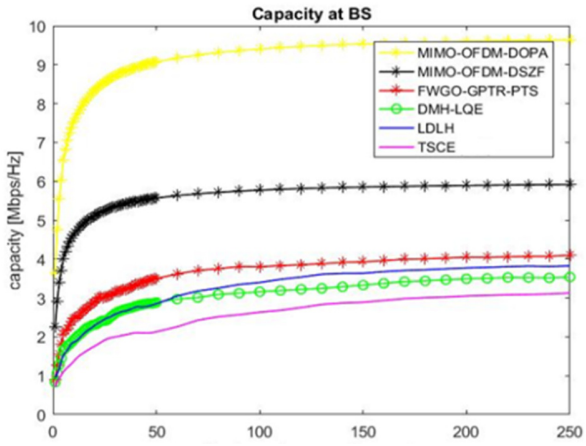

Fig. 10. Capacity achievement of various MIMO-OFDM systems.

Figure 11 shows the transmitted power performance of various MIMO-OFDM systems for 250 UEs. TSCE resulted in 10^{-1} uJ, LDLH had 2×10^{-2} uJ, DMH-LQE had 9×10^{-2} uJ, FWGO-GPTR-PTS had 10^{-3} uJ, and FWGO-GPTR-PTS had 3×10^{-4} uJ of transmitted power. However, the proposed MIMO-OFDM-DOPA exhibited less 9×10^{-4} uJ transmitted power, which was less than the other approaches.

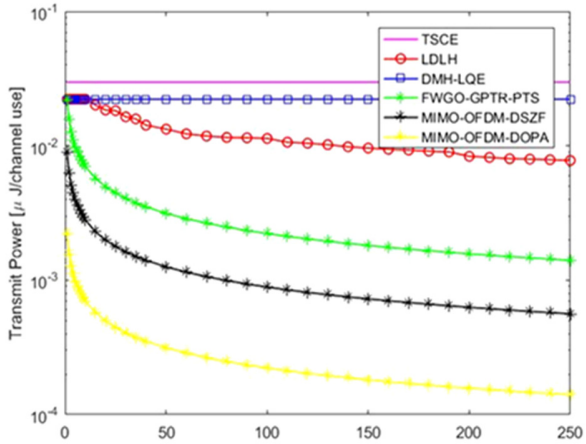

Fig. 11. Transmit power performance of various MIMO-OFDM systems.

IV. CONCLUSION

This study focused on MIMO-OFDM with DSZF equalizer and DOPA-based energy efficiency optimization. MIMO-OFDM reduces pilot contamination. The channel characteristics of the selected pathways are evaluated using the methods provided and interference from surrounding cells within the framework of an undetermined system. By effectively separating channels, the DSZF channel equalizer technique reduces the amount of pilot overhead required. At higher SNR levels, especially at more burdened pilot-contaminated cells, a superior estimate performance was discovered. Then, the DOPA algorithm was used to carry out the well-designed pilot sequence, simultaneously reducing the amount of computing complexity. The comparative findings showed that the proposed method achieved higher energy efficiency and capacity, and reduced BER, MSE, and transmitted power.

With the constant demand for high spectral efficiency and high transmission speed for audio, video, and Internet applications, MIMO-OFDM has become the most fascinating technology for present- and future-generation wireless communications. MIMO-OFDM can achieve high-speed data transmission with improved performance and reliability. By optimizing the use of available resources and using low-power components and algorithms, it is possible to improve energy efficiency and reduce the operational costs associated with wireless communication systems. This makes it possible to use the available bandwidth more efficiently and reduce the amount of energy required for data transmission.

REFERENCES

[1] A. Elsanousi and S. Oztürk, "Performance Analysis of OFDM and OFDM-MIMO Systems under Fading Channels," *Engineering,*

Technology & Applied Science Research, vol. 8, no. 4, pp. 3249–3254, Aug. 2018, https://doi.org/10.48084/etasr.2209.

[2] Z. A. Shamsan, "Statistical Analysis of 5G Channel Propagation using MIMO and Massive MIMO Technologies," *Engineering, Technology & Applied Science Research*, vol. 11, no. 4, pp. 7417–7423, Aug. 2021, https://doi.org/10.48084/etasr.4264.

[3] S. Jothi and A. Chandrasekar, "An Efficient Modified Dragonfly Optimization Based MIMO-OFDM for Enhancing QoS in Wireless Multimedia Communication," *Wireless Personal Communications*, vol. 122, no. 2, pp. 1043–1065, Jan. 2022, https://doi.org/10.1007/s11277-021-08938-7.

[4] C. Panda and U. Bhanja, "Effect of Code and Frequency Index Modulation in MIMO-OFDM-FSO System," *in Optical and Wireless Technologies proceedings of the 4th International Conference on Optical and Wireless Technologies (OWT 2020)*, Jaipur, India, Apr. 2020, pp. 89–95, https://doi.org/10.1007/978-981-16-2818-4_9.

[5] P. R. Kumar, P. V. Naganjaneyulu, and K. S. Prasad, "Partial transmit sequence to improve OFDM using BFO & PSO algorithm," *International Journal of Wavelets, Multiresolution and Information Processing*, vol. 18, no. 1, Jan. 2020, Art. no. 1941018, https://doi.org/10.1142/S0219691319410182.

[6] S. E. El-Khamy, N. O. Korany, and H. Hassan, "A New Efficient Two-Sided Complementary Code Based Channel Estimation Technique 'TSCC-CE' for MIMO-OFDM Systems, Under the Effects of Partial-Band Jamming and Doppler Spread," *IEEE Access*, vol. 9, pp. 155153–155160, 2021, https://doi.org/10.1109/ACCESS.2021.3126553.

[7] Y. Chen, C. Clemente, and J. J. Soraghan, "Partial Fractional Fourier Transform (PFrFT)-MIMO-OFDM for Known Underwater Acoustic Communication Channels," *Information*, vol. 12, no. 11, Nov. 2021, Art. no. 469, https://doi.org/10.3390/info12110469.

[8] C. Reddy and V. Shete, "A Hybrid Linear-Quadratic Estimation (LQE) Technique for Channel Estimation in MIMO-OFDM System," *International Journal of Intelligent Engineering & Systems*, vol. 14, no. 6, pp. 453–463, 2021, https://doi.org/10.22266/ijies2021.1231.40.

[9] W. Raza, X. Ma, A. Ali, A. Raza, and S. Shaikh, "Performance Analysis of Selective Mapping in Underwater Acoustic Orthogonal Frequency Division Multiplexing Communication System," *Engineering, Technology & Applied Science Research*, vol. 11, no. 1, pp. 6696–6702, Feb. 2021, https://doi.org/10.48084/etasr.3941.

[10] K. Ramadan, M. I. Dessouky, and F. E. A. El-Samie, "Modified OFDM configurations with equalization and CFO compensation for performance enhancement of OFDM communication systems using symmetry of the Fourier transform," *AEU - International Journal of Electronics and Communications*, vol. 126, Nov. 2020, Art. no. 153247, https://doi.org/10.1016/j.aeue.2020.153247.

[11] J. Mestoui, M. El Ghzaoui, M. Fattah, A. Hmamou, and J. Foshi, "Performance analysis of CE-OFDM-CPM Modulation using MIMO system over wireless channels," *Journal of Ambient Intelligence and Humanized Computing*, vol. 11, no. 10, pp. 3937–3945, Oct. 2020, https://doi.org/10.1007/s12652-019-01628-0.

[12] J. Simon, "A Performance Analysis of Wavelet based LTE-OFDM with Multi-equalizers," *Turkish Journal of Computer and Mathematics Education (TURCOMAT)*, vol. 12, no. 6, pp. 108–116, Apr. 2021.

[13] K. Chen-Hu, Y. Liu, and A. G. Armada, "Non-Coherent Massive MIMO-OFDM Down-Link Based on Differential Modulation," *IEEE Transactions on Vehicular Technology*, vol. 69, no. 10, pp. 11281–11294, Jul. 2020, https://doi.org/10.1109/TVT.2020.3008913.

[14] J. Kassam *et al.*, "Two-Step Multiuser Equalization for Hybrid mmWave Massive MIMO GFDM Systems," *Electronics*, vol. 9, no. 8, Aug. 2020, Art. no. 1220, https://doi.org/10.3390/electronics9081220.

[15] I. Aldaya *et al.*, "Compensation of nonlinear distortion in coherent optical OFDM systems using a MIMO deep neural network-based equalizer," *Optics Letters*, vol. 45, no. 20, pp. 5820–5823, Oct. 2020, https://doi.org/10.1364/OL.403778.

[16] D. S. Kapoor and A. K. Kohli, "Intelligence-based Channel Equalization for 4x1 SFBC-OFDM Receiver," *Intelligent Automation & Soft Computing*, vol. 26, no. 3, pp. 439–446, 2020, https://doi.org/10.32604/iasc.2020.013920.

[17] S. Nandi, N. N. Pathak, and A. Nandi, "A Novel Adaptive Optimized Fast Blind Channel Estimation for Cyclic Prefix Assisted Space–Time Block Coded MIMO-OFDM Systems," *Wireless Personal Communications*, vol. 115, no. 2, pp. 1317–1333, Nov. 2020, https://doi.org/10.1007/s11277-020-07629-z.

[18] S. Nandi, N. N. Pathak, and A. Nandi, "Avenues to Improve Channel Estimation Using Optimized CP in STBC Coded MIMO-OFDM Systems—A Global Optimization Approach," in *Proceeding of Fifth International Conference on Microelectronics, Computing and Communication Systems*, Ranchi, India, 2021, pp. 249–259, https://doi.org/10.1007/978-981-16-0275-7_21.

[19] N. H. Cheng, K. C. Huang, Y. F. Chen, and S. M. Tseng, "Maximum likelihood-based adaptive iteration algorithm design for joint CFO and channel estimation in MIMO-OFDM systems," *EURASIP Journal on Advances in Signal Processing*, vol. 2021, no. 1, Jan. 2021, Art. no. 6, https://doi.org/10.1186/s13634-020-00711-5.

[20] R. Ayeswarya and N. A. Prabha, "Fractional Wavelet Transform based PAPR Reduction Schemes in Multicarrier Modulation System," *IETE Journal of Research*, vol. 68, no. 1, pp. 732–742, Jan. 2022, https://doi.org/10.1080/03772063.2019.1621685.

[21] R.Shivaji *et al.*, "Implementation of an Effective Hybrid PTS Model for PAPR in MIMO-OFDM System," in *Proceedings of the 2nd International Conference on Data Science Machine Learning and Applications: ICDSMLA 2020*, Pune, India, 2020.